PLOS COMPUTATIONAL BIOLOGY

RESEARCH ARTICLE

Gain control with A-type potassium current: I_A as a switch between divisive and subtractive inhibition

Joshua H. Goldwyn[1]*, Bradley R. Slabe[2], Joseph B. Travers[3], David Terman[2]

1 Department of Mathematics and Statistics, Swarthmore College, Swarthmore, Pennsylvania, United States of America, **2** Department of Mathematics, The Ohio State University, Columbus, Ohio, United States of America, **3** Division of Biosciences, College of Dentistry, The Ohio State University, Columbus, Ohio, United States of America

* jhgoldwyn@gmail.com

Citation: Goldwyn JH, Slabe BR, Travers JB, Terman D (2018) Gain control with A-type potassium current: I_A as a switch between divisive and subtractive inhibition. PLoS Comput Biol 14(7): e1006292. https://doi.org/10.1371/journal.pcbi.1006292

Editor: Brent Doiron, University of Pittsburgh, UNITED STATES

Received: February 14, 2018

Accepted: June 11, 2018

Published: July 9, 2018

Data Availability Statement: All relevant data are within the paper and its Supporting Information files.

Funding: This work was partially supported by the National Science Foundation award DMS1410935 (http://www.nsf.gov) to DT and the National Institute on Deafness and Other Communication Disorders award R01DC016112 (http://www.nidcd.nih.gov/) to JT and DT. The funders had no role in study design, data collection and analysis, decision to publish, or preparation of the manuscript.

Abstract

Neurons process and convey information by transforming barrages of synaptic inputs into spiking activity. Synaptic inhibition typically suppresses the output firing activity of a neuron, and is commonly classified as having a *subtractive* or *divisive* effect on a neuron's output firing activity. Subtractive inhibition can narrow the range of inputs that evoke spiking activity by eliminating responses to non-preferred inputs. Divisive inhibition is a form of gain control: it modifies firing rates while preserving the range of inputs that evoke firing activity. Since these two "modes" of inhibition have distinct impacts on neural coding, it is important to understand the biophysical mechanisms that distinguish these response profiles. In this study, we use simulations and mathematical analysis of a neuron model to find the specific conditions (parameter sets) for which inhibitory inputs have subtractive or divisive effects. Significantly, we identify a novel role for the A-type Potassium current (I_A). In our model, this fast-activating, slowly-inactivating outward current acts as a switch between subtractive and divisive inhibition. In particular, if I_A is strong (large maximal conductance) and fast (activates on a time-scale similar to spike initiation), then inhibition has a subtractive effect on neural firing. In contrast, if I_A is weak or insufficiently fast-activating, then inhibition has a divisive effect on neural firing. We explain these findings using dynamical systems methods (plane analysis and fast-slow dissection) to define how a spike threshold condition depends on synaptic inputs and I_A. Our findings suggest that neurons can "self-regulate" the gain control effects of inhibition via combinations of synaptic plasticity and/or modulation of the conductance and kinetics of A-type Potassium channels. This novel role for I_A would add flexibility to neurons and networks, and may relate to recent observations of divisive inhibitory effects on neurons in the nucleus of the solitary tract.

Author summary

Neurons process information by generating spikes in response to two types of synaptic inputs. Excitatory inputs increase spike rates and inhibitory inputs decrease spike rates

Competing interests: The authors have declared that no competing interests exist.

(typically). The interaction between these two input types and the transformation of these inputs into spike outputs is not, however, a simple matter of addition and subtraction. Inhibitory inputs can suppress outputs in a variety of ways. For instance, in some cases, inhibition adjusts the rate of spiking activity while preserving the range of inputs that evoke spiking activity; an important computational principle known as gain control. We use simulations and mathematical analysis of a neuron model to identify properties of a neuron that determine how inhibitory inputs affect spiking activity. Specifically, we demonstrate how the gain control effects of inhibition depend on the A-type Potassium current. This novel role for the A-type Potassium current provides a way for neurons to flexibly regulate how they process synaptic inputs and transmit signals to other areas of the brain.

Introduction

The activity of a neuron is driven by barrages of synaptic inputs. Synaptic inputs are classified as either excitatory (those that promote spike generation) and inhibitory (those that impede spike generation). The interplay between these two "opposing" inputs influences how neurons process and transmit information in the brain.

To characterize the nature of inhibition, researchers often distinguish between inhibition that has a *subtractive* effect on neural firing, versus inhibition that has a *divisive* effect [1]. Inhibition is said to be subtractive if it reduces the firing activity of a neuron by (roughly) a constant amount, regardless of the strength or amount of synaptic excitation. Inhibition is said to be divisive if it reduces the firing activity of a neuron by an amount that is (roughly) proportional to the neuron's firing rate. We illustrate this distinction in Fig 1, by showing output firing rate of a neuron as a function of the rate of its excitatory inputs (not actual data).

The differences between these modes of inhibition has important consequences for neural coding. Subtractive inhibition suppresses responses to "non-preferred" stimuli that evoke infrequent responses in the absence of inhibition. This can be useful for promoting the representation of "preferred" inputs. In contrast, divisive inhibition is a mechanism for neural gain

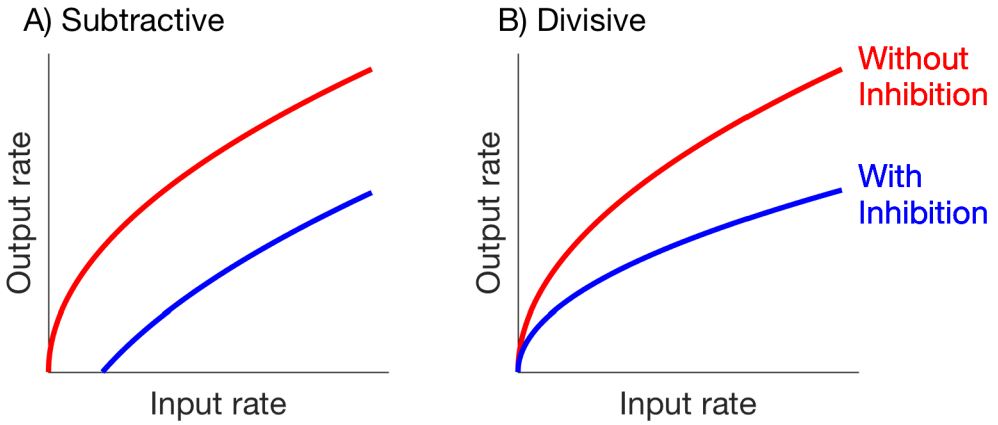

Fig 1. Comparison of firing rate input/output relations for subtractive and divisive inhibition (illustration only, not actual data). A: Subtractive inhibition: output rate without inhibition is $r_{out} = \sqrt{r_{in}}$, and output rate with inhibition is $r_{out} = \sqrt{r_{in}} - c$, where c is a constant with $c > 0$. **B**: Divisive inhibition: output rate without inhibition is $r_{out} = \sqrt{r_{in}}$ (same as in **A**), and output rate with with inhibition is $\alpha\sqrt{r_{in}}$, where α is a constant with $0 < \alpha < 1$.

https://doi.org/10.1371/journal.pcbi.1006292.g001

control: it reduces the firing rate of a neuron while preserving the overall range of inputs to which the neuron is responsive [2]. Understanding the physiological mechanisms that determine how and why inhibition acts in these two modes is key for understanding how neurons and networks function. Past studies have identified numerous possibilities for mechanisms underlying these two modes of inhibition, including the stochastic (noisy) nature of synaptic inputs [3], the balance between excitatory and inhibitory inputs [4], shunting inhibition [5, 6], synaptic depression [7], and circuit structure [2, 8], and see [1] for additional review.

In this study, we identify a novel role for A-type voltage-gated potassium current in determining whether inhibition acts in a subtractive or divisive manner. Voltage-gated K^+ channels play an important role in regulating neuronal excitability [9, 10]. Here, we focus on the class of K^+ channels that produce an A-type current [11]. These outward currents are mediated by a variety of membrane-bound channels [12–14], found primarily on dendrites [15] but with a somatic location in some cells [16, e.g.]. A-type currents vary greatly in their voltage dependence and kinetics. Although a limited number of channels are typically open (active) at the resting membrane potential, producing a "window current" [17, 18], additional hyperpolarization further "primes" [19] or de-inactivates the membrane [20], making more channels available for activation by a depolarizing stimulus. Thus, the magnitude of A-type currents are particularly sensitive to inhibitory inputs. Inactivation kinetics vary greatly, ranging from less than 20 ms to as much as 600 ms, even within populations of neurons sharing a single potassium channel subfamily [14, e.g.].

Through mathematical analysis and simulations, we explore the combined effects of synaptic inputs and voltage-gated ion currents on spiking dynamics of a neuron model. We find that if the A-type current is sufficiently large and activates rapidly, then it combines with inhibitory inputs to suppress firing activity in a subtractive manner. If, instead, the A-current is sufficiently weak or activates slowly (relative to spike initiation dynamics), then inhibition has a divisive effect on firing rates. Our work identifies a route through which adaptive or dynamic changes to the intrinsic dynamics of neurons (for example, through modification of ion currents [21]) can modulate the effects of inhibition. This capability for individual neurons to switch between different inhibition "regimes" could provide useful flexibility to neural systems.

Materials and methods

We simulate and analyze two models of neural dynamics. The first is a one-compartment model that approximates a neuron as a single, isopotential unit (a "point neuron" model). The second is a multi-compartment model that includes a region of voltage-gated currents attached to a spatially-extended region of passive membrane ("soma" and "dendrite" regions, respectively). We describe these models below.

One-compartment neuron model

The dynamics of membrane potential, V, in the one-compartment neuron model are

$$CV' = -I_L - I_K - I_A - I_{Na} - I_{Syn,E} - I_{Syn,I} \tag{1}$$

where the membrane capacitance is $C = 1\ \mu\text{F/cm}^2$. Here, and throughout, we use V' to indicate the time-derivative of V, i.e. dV/dt. The ionic currents (leak, potassium, A-type potassium, and sodium) are given by the equations

$$\begin{aligned} I_L &= g_L(V - V_L), & I_K &= g_K n^4 (V - V_K), \\ I_A &= g_A a^3 b (V - V_K), & I_{Na} &= g_{Na} m^3 h (V - V_{Na}). \end{aligned} \tag{2}$$

We use the following fixed parameter values for maximal conductances: $g_L = 1$ mS/cm^2, $g_K = 45$ mS/cm^2, and $g_{Na} = 37$ mS/cm^2. We use a range of values for the maximal conductance of the A-current (g_A) to observe transitions between subtractive and divisive effects of inhibition. The reversal potentials are $V_L = -70$ mV, $V_K = -80$ mV, and $V_{Na} = 55$ mV.

We make several simplifications, similar to those first suggested in [22], to the gating variables in the model. We identify sodium activation as a fast process and assume it evolves instantaneously to its voltage-dependent steady-state value. That is, we let $m = m_\infty(V) = 1/(1 + e^{-(V+30)/15})$. In addition, we observe an approximately linear relationship between sodium inactivation and potassium inactivation and thus set $h = 1 - n$.

The remaining gating variables are n, a, and b. Their dynamics are described by equations of the form

$$X' = \phi_X \frac{X_\infty(V) - X}{\tau_X(V)}, \qquad X = n, a, b. \tag{3}$$

The voltage-dependent steady-state functions are of the form $X_\infty(V) = 1/(1 + e^{(X-\theta_X)/\sigma_X})$. For the potassium activation variable, n, we assume that $\phi_n = 0.75$, $\theta_n = -32$ and $\sigma_n = -8$. The time-scale for the n variable is voltage-dependent: $\tau_n(V) = 1 + 100/(1 + e^{(V+80)/26})$. Similar to the model presented in [23], we assume that $\phi_a = 1$, $\theta_a = -50$ and $\sigma_a = 20$ for A-type potassium activation, and $\phi_b = 1$, $\theta_b = -70$ and $\sigma_b = -6$ for A-type potassium inactivation. The time-scales for the A-type current are constants: $\tau_a = 2$ ms and $\tau_b = 150$ ms.

Inputs to the model include synaptic excitation ($I_{Syn,E}$) and inhibition ($I_{Syn,I}$). Excitatory current is $I_{Syn,E} = g_{Syn,E}\, s_E(V - V_E)$ and inhibitory current is given by an analogous equation. The maximal excitatory and inhibitory conductances ($g_{Syn,E}$ and $g_{Syn,I}$) are parameters that we vary in simulations. The reversal potentials are $V_E = 0$ mV for excitation and $V_I = -85$ mV for inhibition. The gating variables, s_E and s_I, reset to one at the time of a synaptic event and decay with an exponential time-course. That is, the excitatory gating variable is defined as

$$s_E(t) = \begin{cases} 1 & \text{if } t = t_E \\ e^{-\beta_E(t-t_E)} & \text{if } t > t_E \end{cases} \tag{4}$$

where t_E is the time of the most recent excitatory event and the decay time constant is $\beta_E = 0.2$ ms^{-1}. A similar equation holds for the inhibitory gating variable s_I, but with a time constant $\beta_I = 0.18$ ms^{-1}. Excitatory event times are randomly distributed according to a homogeneous Poisson process with rate r_E. Inhibitory event times are periodic with rate r_I. We vary the values of the rate parameters (r_E, r_I) in our investigations. Our choice of these input patterns simplifies some of our mathematical analysis. In addition, our choice of periodic inhibitory events was motivated by the design of *in vitro* experiments, presented in [24], in which inhibitory interneurons were activated periodically using optogenetic techniques. In additional simulations included as S1 and S2 Figs we allowed the timing of inhibitory inputs to be random with event times drawn from a homogeneous Poisson process. We did not observe substantially different results in simulations that used these non-periodic inhibitory inputs.

Multi-compartment neuron model

In some simulations we augment the one-compartment (point neuron) model by attaching additional compartments that represent a dendritic process. We assume that the dendrite consists of nine equally-sized compartments. Moreover, the neuron receives inhibitory input at its soma (the first compartment) and excitatory input at a dendritic compartment.

Voltage in the first compartment (soma) is denoted V_1 and is given by Eq 1 with synaptic excitation removed and with a new term representing the flow of current between compartments (axial current):

$$CV_1' = -I_{L,1} - I_K - I_A - I_{Na} - I_{Ax,1} - I_{Syn,I}. \quad (5)$$

The remaining dendritic compartments do not include potassium, A-type potassium, or sodium currents, and thus V_j for $2 \leq j \leq 10$ follows the linear dynamics of a passive cable:

$$CV_j' = \begin{cases} -I_{L,j} - I_{Ax,j} - I_{Syn,E} & \text{at location of excitatory inputs} \\ -I_{L,j} - I_{Ax,j} & \text{at other locations.} \end{cases} \quad (6)$$

Leak conductance in the dendrite compartments is $g_L = 0.1$ mS/cm^2 (one-tenth the value in the first compartment). Axial current is

$$I_{Ax,j} = \begin{cases} g_{Ax}(V_1 - V_2) & \text{for } j = 1 \\ g_{Ax}(-V_{j-1} + 2V_j - V_{j+1}) & \text{for } 2 \leq j \leq 9 \\ g_{Ax}(V_{10} - V_9) & \text{for } j = 10 \end{cases} \quad (7)$$

where $g_{Ax} = 10$ mS/cm^2.

Input currents are defined in a manner identical to inputs in the one-compartment model. Excitatory and inhibitory gating variables follow Eq 4. Excitatory synaptic event times are drawn from a homogeneous Poisson process with rate r_E and inhibitory synaptic event times are periodic with rate r_I. These constants, as well as synaptic input strengths ($g_{Syn,E}$, $g_{Syn,I}$) and the compartment targeted by the excitatory inputs, are parameters we vary in our investigations.

Computations

We simulated the point-neuron and multi-compartment neuron models using software written in the C computer programming language. We integrated differential equations using the fourth order implicit Runge-Kutta method available in the GNU scientific library. We also simulated the one-compartment model and a reduced model version of the one-compartment using XPPAUT, and performed bifurcation analysis of these models using the AUTO feature of XPPAUT [25]. Simulation code is available for download at https://github.com/jhgoldwyn/Gain-Control-With-IA.

Results

Examples of divisive and subtractive inhibition

We first study the relationship between excitatory input rate (r_E) and firing output rate (r_{out}) of the one-compartment model. In Fig 2A, we plot examples of this input/output relationship for simulations without inhibition (empty circles, $g_{Syn,I} = 0$) and with inhibition (filled circles, $g_{Syn,I} = 1$). The A-channel conductance in these simulations is $g_A = 20$ mS/cm^2. For these parameters, we observe that inhibition reduces the model neuron's output firing rate, but the neuron continues to fire in response to arbitrarily low input rates.

An additional way to view the effect of inhibition is to plot output firing rates in the presence of inhibition as a function of output firing rates in the absence of inhibition, as we have done in Fig 2C. There is a roughly linear relationship between these output firing rates, which

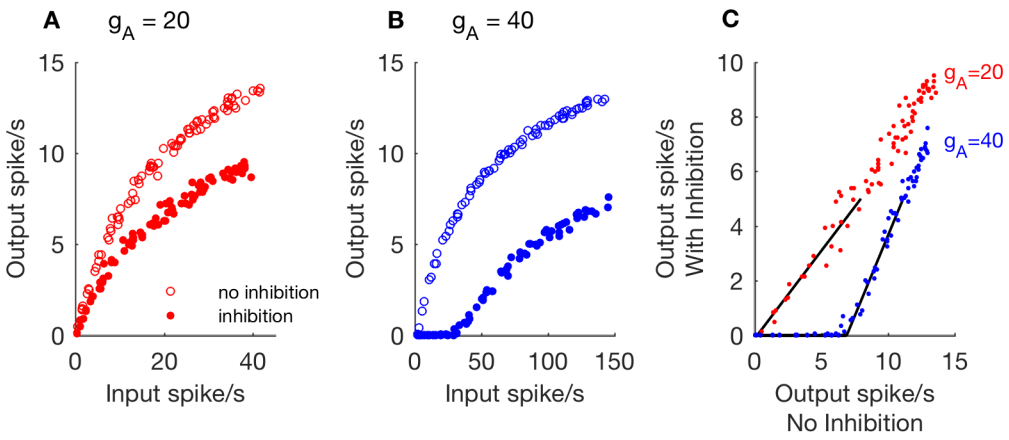

Fig 2. Examples of divisive and subtractive effects of inhibition in the one-compartment model. A, B: Output firing rates as a function of excitatory input rate, computed from simulations without inhibition (empty circles, $g_{Syn,I} = 0$) and with inhibition (filled circles, $g_{Syn,I} = 1$ and $r_I = 50$ Hz). Excitatory synaptic strength is $g_{Syn,E} = 0.5$. In **A**: Divisive rescaling of the input/output relation with $g_A = 20$. In **B**: Subtractive shifting of the input/output relation with $g_A = 40$. **C**: Data from **A** and **B** are replotted with output firing rates in the absence of inhibition on the ordinate and output firing rates in the presence of inhibition on the abscissa. Threshold-linear functions are fit to simulation data (black lines). Rightward shift of threshold-linear function for $g_A = 40$ is characteristic of subtractive inhibition.

https://doi.org/10.1371/journal.pcbi.1006292.g002

we describe by fitting these data with a threshold-linear function of the form

$$y = [m(x - x_0)]_+ \tag{8}$$

where the symbol $[\cdot]_+$ indicates we set $y = 0$ if the argument $m(x - x_0)$ is negative. We obtain the slope parameter m and the x-intercept parameter x_0 by applying a curve-fitting procedure (using the *fminsearch* command in MATLAB) to the portion of data for which the output firing rate in the presence of inhibition is less than five spikes per second. In this example, inhibition affects the value of the slope parameter m, but the value of x_0 is nearly zero. We identify responses with these characteristics as cases in which the effect of inhibition is *divisive*.

In Fig 2B, we increase the A-channel conductance to $g_A = 40$ mS/cm^2. We observe that inhibition has a different effect on the input/output curve in these simulations. In the presence of inhibition (filled circles), there is now a non-zero value of the input rate below which the neuron model does not spike ($r_{out} = 0$ for $r_E \lessapprox 30$). Moreover, when we view the relationship between output firing rates with and without inhibition in Fig 2C, we observe a rightward shift of the threshold-linear function fit to these data (positive-valued x-intercept). We identify responses with these characteristics as cases in which the effect of inhibition is *subtractive*.

Although we refer throughout to the effect of inhibition on responses as being either divisive or susbtractive, this is a simplification of a more complicated and subtle reality. In fact, responses can show characteristics of both divisive and subtractive inhibition. In particular, the input/output curves can be right-shifted (evidence of subtractive inhibition) and have slopes that are decreased relative to slopes for $g_A = 0$ (evidence of divisive inhibition). We provide evidence of such "mixed" responses in S3 Fig. To be clear: we refer to scenarios in which the input/output curves have only a change of slope as *divisive*, and scenarios in which the input/output curve is right-shifted as *subtractive*. In other words, the subtractive case will also include "mixed" responses.

Parameter study: Inhibition is subtractive for strong A-current conductance or weak excitatory conductance

We identify two parameters in the one-compartment model that are key factors in determining whether inhibition has a divisive or subtractive effect on firing rate responses: the A-channel conductance (g_A) and the excitatory synaptic conductance ($g_{Syn,E}$). In Fig 3A we show a set of threshold-linear functions computed using $g_A = 20$, 30 and 40, and synaptic excitation strength fixed at $g_{Syn,E} = 0.5$. The transition from divisive to subtractive inhibition is evident in the rightward shift of these threshold-linear functions with increasing values of g_A. This transition occurs, for this parameter set, for $g_A \approx 33$, a point we investigate in more detail below, with simulations and phase plane analysis.

In Fig 3B, we show a set of threshold-linear functions with $g_A = 30$ fixed, but now varying the value of $g_{Syn,E}$ from 0.4 to 0.7. The stronger excitatory inputs ($g_{Syn,E} = 0.5$, 0.7) cause inhibition to have a divisive effect, while the weaker excitatory input ($g_{Syn,E} = 0.4$) causes inhibition to have a subtractive effect. In these simulations, we do not vary the parameters associated with inhibition. They are $g_{Syn,I} = 1$ and $r_I = 50$ Hz.

From these simulations, we conclude that the effect of inhibition on firing rates in the one-compartment model can switch from divisive to subtractive for sufficiently strong A-current conductance or sufficiently weak excitatory synaptic conductance. In the parameter plane of g_A and $g_{Syn,E}$, then, there is a boundary that separates parameter sets that produce divisive inhibition from parameter sets that produce subtractive inhibition. We map this boundary by performing simulations throughout the (g_A, $g_{Syn,E}$) parameter space. For each simulation, we fit threshold-linear functions to characterize the relationship between output firing rates in the presence and absence of inhibition. We then find the smallest value of g_A for which the x-intercept of the threshold-linear function is right-shifted by more than two spikes per second and label this as boundary between subtractive and divisive inhibition.

In Fig 4, we show the results of this parameter exploration. We performed these simulations and classification procedure for several values of inhibition conductance strength (varying

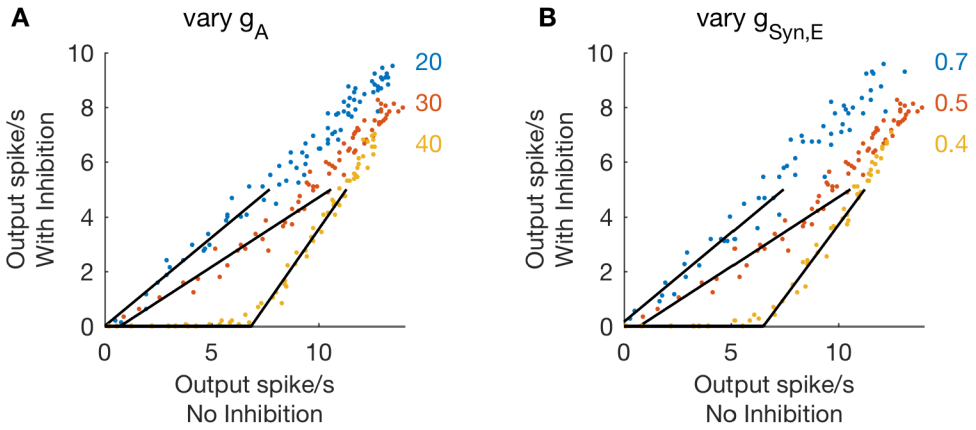

Fig 3. Inhibition is subtractive for large A-channel conductance or weak synaptic excitation. A, B: Firing rates computed from simulations with inhibition ($g_{Syn,I} = 1$, $r_I = 50$ Hz, abscissa) plotted as a function of firing rates computed from simulations without inhibition ($g_{Syn,I} = 0$, ordinate). In **A**: Three values of A-channel conductance are compared ($g_A = 20$, 30, 40) with synaptic excitation strength fixed at $g_{Syn,E} = 0.5$. Inhibition is subtractive for large g_A evident in the rightward shift of the threshold-linear relationship between firing rates for $g_A = 40$. In **B**: Three values of synaptic excitation strength are compared ($g_{Syn,E} = 0.4$, 0.5, 0.7) with A-channel conductance fixed at $g_A = 30$. Inhibition is subtractive for weaker excitation, evident in the rightward shift of the threshold-linear relationship between firing rates for $g_{Syn,E} = 0.4$.

https://doi.org/10.1371/journal.pcbi.1006292.g003

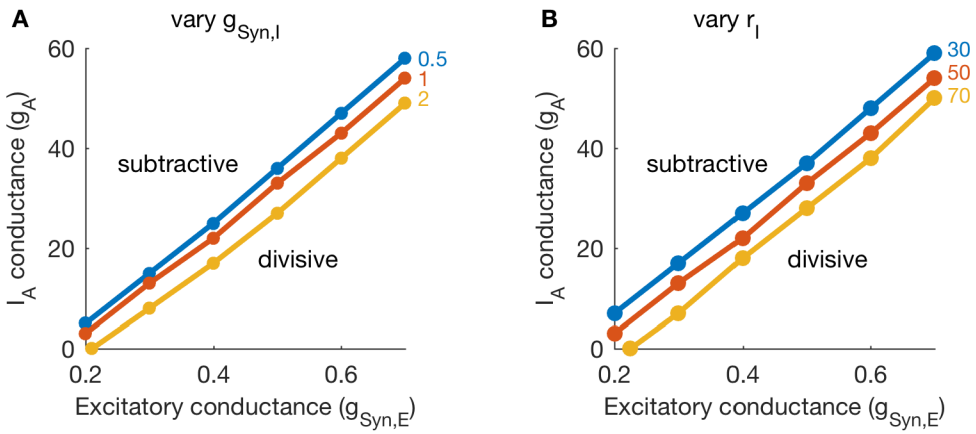

Fig 4. Boundary between subtractive and divisive inhibition in ($g_{Syn,E}$, g_A) parameter space. A, B: For each parameter set, we fit threshold-linear functions to characterize the relationship between output firing rates in the presence and absence of inhibition. Dots in each panel identify the smallest value of g_A (for a given parameter set) at which inhibition is subtractive. In **A**: We vary inhibition strength ($g_{Syn,I}$ = 0.5, 1, 2) and keep inhibition rate fixed at 50 Hz. In **B**: We vary inhibition rate (r_I = 30, 50, 70 Hz) and keep inhibition strength fixed at $g_{Syn,I}$ = 1. The values of g_A that define the boundary between subtractive and divisive inhibition decrease with increases in either inhibition parameter ($g_{Syn,I}$ or r_I).

https://doi.org/10.1371/journal.pcbi.1006292.g004

values of $g_{Syn,I}$, in Fig 4A), and for several values of inhibition rate (varying values of r_I, in Fig 4B). The lines in each panel separate parameter regions for which inhibition is divisive (lower right corners in each panel) from parameter regions in which inhibition is subtractive. This confirms our earlier observation that the effect of inhibition is subtractive if A-channel conductance is sufficiently strong or excitatory inputs are sufficiently weak.

These simulations also demonstrate that inhibition parameters modify (weakly) the location of the boundary between divisive and subtractive inhibition in the (g_A, $g_{Syn,E}$) parameter plane. Stronger inhibition (either through larger $g_{Syn,I}$ or larger r_I values) decreases the portion of the (g_A, $g_{Syn,E}$) parameter plane in which inhibition has a divisive effect on firing rate responses.

Analysis of a reduced one-compartment model

We use mathematical analysis to derive the parameter regions in which the model exhibits either a divisive or subtractive response to inhibition. We begin by considering a reduced model in which activation of the A-current is instantaneous; that is, $a = a_\infty(V)$. Later, we discuss how the model's response to inhibition may change if this assumption does not hold.

Excitability analysis using fast/slow dissection. A first step in the analysis is to determine under what conditions the neuron will fire an action potential in response to an excitatory input. An important distinction between divisive and subtractive inhibition is whether the neuron can respond to arbitrarily low excitatory input rates. We analyze the model by viewing solutions in the (V, n) phase plane. A major challenge in this approach is that the phase plane depends not only on the other dependent variable, b, but on the values of the synaptic inputs, s_E and s_I. Suppose, for the time being, that these variables are fixed constants. Fig 5 shows phase planes for different values of these constants. In particular, it illustrates how the V-nullclines change as b, s_E, s_I and the parameter g_A changes. In each case, the V-nullcline has left, middle and right branches, while the n-nullcline is a monotone increasing function. Note that values of n along the V-nullcline are increasing functions of s_E and decreasing functions of b, s_I and g_A.

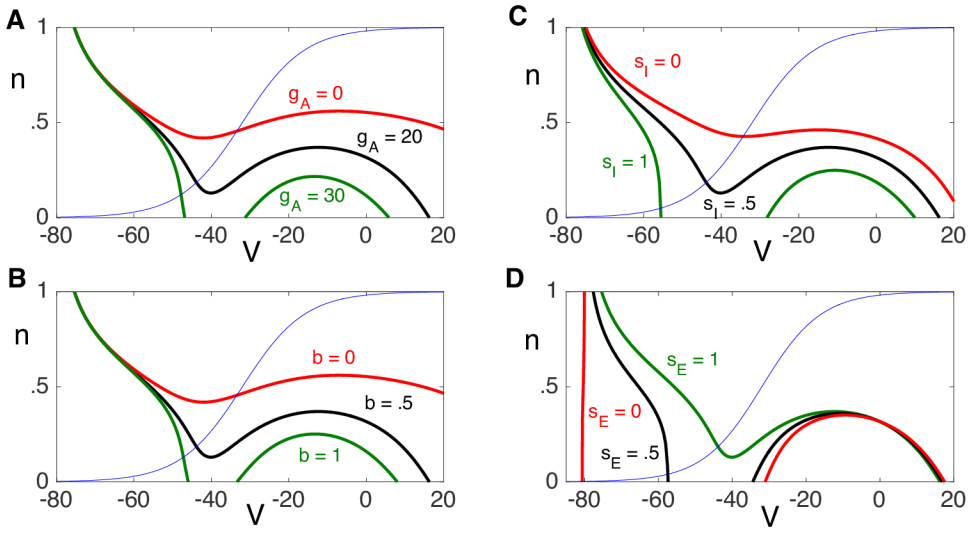

Fig 5. Dependence of the V-nullcline on A: g_A, B: b, C: s_I and D: s_E. Default values of the parameters are $g_A = 20$, $b = .5$, $s_I = .5$ and $s_E = 1$. Moreover, $g_{Syn,E} = 3$ and $g_{Syn,I} = 5$. Thin blue line is $n_\infty(V)$, the n-nullcline.

https://doi.org/10.1371/journal.pcbi.1006292.g005

We consider V to be a fast variable and n and b to be slow variables. During silent or active phases, solutions lie on, respectively, the left or right branch of the V-nullcline corresponding to values of b, s_E and s_I. The jumps up and down of action potentials correspond to horizontal transitions between left and right branches in the phase plane.

Now suppose that the solution initially lies in the silent phase along the left branch of some V-nullcline and there is an excitatory synaptic input. Then s_E will immediately jump from $s_E = 0$ to $s_E = 1$, resulting in an immediate change in the V-nullcline, as shown in Fig 5D. If $(V(0), n(0))$ lies below the left knee of this new $s_E = 1$, V-nullcline, then the solution will jump to the right branch of the new V-nullcline, resulting in an action potential. However, if $(V(0), n(0))$ lies above this left knee, then the solution will jump to the left branch of the new V-nullcline; that is, the solution will not respond to the excitatory input with an action potential.

This discussion helps to explain when the neuron will or will not fire an action potential in response to an excitatory input. In particular, there are two reasons why the neuron may not respond and these are illustrated in Fig 6. The first reason is that the neuron may be in a refractory period. That is, if the excitatory input arrives shortly after the neuron has previously fired,

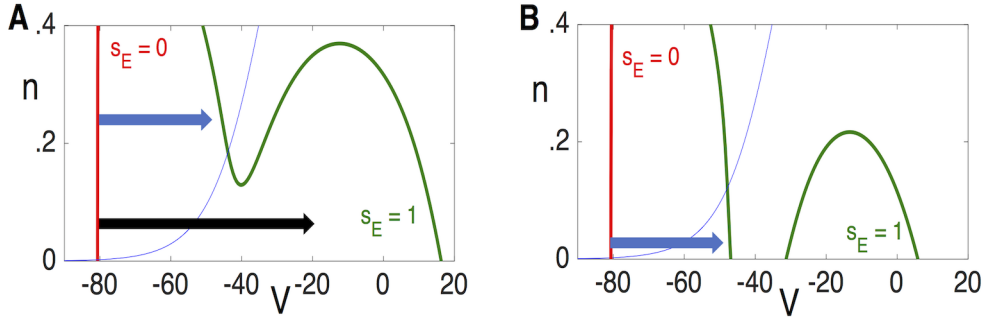

Fig 6. Response to an excitatory input. A. The neuron will or will not fire an action potential if, at the time of the excitatory input, it lies below or above the left knee of the $s_E = 1$ cubic, respectively. **B.** The neuron cannot respond with an action potential if the left knee of the $s_E = 1$ cubic lies below the $n = 0$ axis.

https://doi.org/10.1371/journal.pcbi.1006292.g006

then the K^+ activation variable, n, may not have had enough time to recover and evolve below the left knee of the $s_E = 1$ cubic nullcline. The second reason is that the inhibitory input, s_I, may be too strong and the left knee of the $s_E = 1$ cubic may lie below the $n = 0$ axis. In this case, the neuron will not respond even though there has been a long time since the preceding excitatory input.

Estimate of b. One difficulty is that the cubic nullclines depend on the time-dependent variable b. For the analysis, we replace b by its average value along solutions, which we estimate as follows. A key observation is that the average value of b can be well approximated by considering a model consisting only of synaptic inputs and the leak current. In particular, to compute the average value of b we may ignore the voltage dependent Na^+, K^+ and A-currents.

To justify this claim, we first simulate the full model for different values of g_A and r_E, and then compute the average value of b along solutions, which we denote as $b_{av}(r_E, g_A)$. Fig 7A shows plots of b_{av} versus r_E for different values of g_A. Note that b_{av} depends only weakly on g_A and is a decreasing function of r_E.

We next repeat these simulations with $g_A = g_K = g_{Na} = 0$. Actually, we perform the simulations twice: once with purely excitatory inputs ($r_I = 0$) and then with purely inhibitory inputs ($r_E = 0$). This gives rise to a curve $\hat{b}_E(r_E)$ and a constant $\hat{b}_I$. We then let

$$\hat{b}_{av}(r_E) = \hat{b}_I + \hat{b}_E(r_E) - \hat{b}_E(0).$$

Fig 7B shows that $\hat{b}_{av}(r_E)$ gives an excellent approximation of $b_{av}(r_E, g_A)$.

We can simplify the anaysis further by considering a fast/slow reduction with V as the fast variable. If $g_A = g_K = g_{Na} = 0$, then V satisfies the *linear* equation:

$$V' = -g_L(V - V_L) - g_{Syn,E}\, s_E\, (V - V_{Syn,E}) - g_{Syn,I}\, s_I\, (V - V_{Syn,I}).$$

Treating V as a fast variable, we set the right hand side of this equation equal to 0 and solve for V to obtain

$$V = \frac{g_L\, V_L + g_{Syn,E}\, s_E\, V_{Syn,E} + g_{Syn,I}\, s_I\, V_{Syn,I}}{g_L + g_{Syn,E}\, s_E + g_{Syn,I}\, s_I}. \tag{9}$$

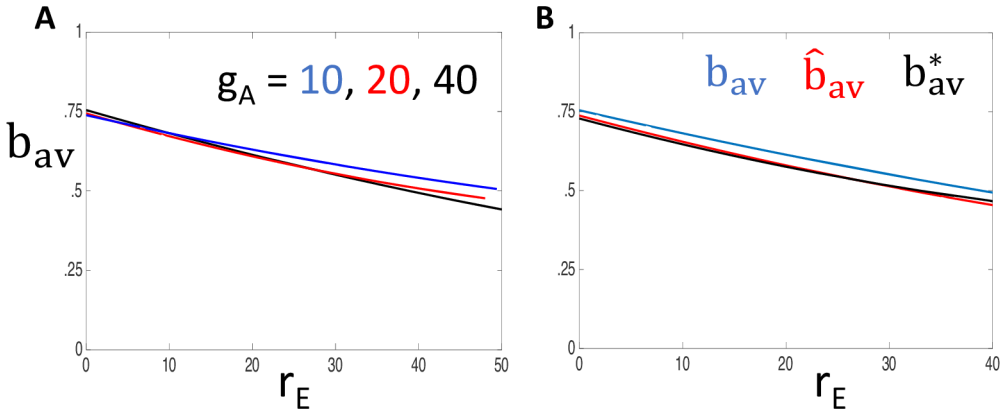

Fig 7. Approximation of *b* (a slow variable) by its average value. A: Plots of b_{av} vs. r_E for different values of g_A. **B**: Plots of $\hat{b}_{av}(r_E)$, $b^*_{av}(r_E)$ and $b_{av}(r_E, g_A)$ with $g_A = 40$. In both panels, $g_{Syn,E} = 3$, $g_{Syn,I} = 5$ and $r_I = 50$ Hz.

https://doi.org/10.1371/journal.pcbi.1006292.g007

As before, we treat excitatory inputs and inhibitory inputs separately. Let

$$V_E = \frac{g_L V_L + g_{Syn,E} s_E V_{Syn,E}}{g_L + g_{Syn,E} s_E} \quad \text{and} \quad V_I = \frac{g_L V_L + g_{Syn,I} s_I V_{syn,I}}{g_L + g_{Syn,I} s_I}.$$

Then let $b_E^*(r_E, t)$ and $b_I^*(t)$ be solutions to Eq 3 with $X = b$, and $V = V_E$ and $V = V_I$, respectively. Finally, let $b_E^*(r_E)$ and b_I^* be the average values of b_E^* and b_I^* along solutions and set

$$b_{av}^*(r_E) = b_I^* + b_E^*(r_E) - b_E^*(0).$$

Fig 7B shows that $b_{av}^*(r_E)$ gives an excellent approximation of $\hat{b}_{av}(r_E)$. In the analysis that follows, we replace the dependent variable b by constants $b_{av}^*(r_E)$.

The left knee. Our previous discussion emphasized the importance of the left knees of the cubic-shaped V-nullclines when $s_E = 1$. If this left knee lies below the $n = 0$ axis, then the neuron cannot spike in response to an excitatory input. For the reduced model, with $a = a_\infty(V)$, this left knee depends on the values of s_I, b and g_A. Here, we replace b by $b_{av}^*(r_E)$ and denote the value of n at the left knee as $N_{lk}(s_I, r_E, g_A)$. We compute the positions of the left knees using XPPAUT.

Identification of inhibition as divisive or subtractive. By computing the position of the left knee, we can determine for which parameter values inhibition will have a divisive effect and for which values it will have a subtractive effect. Let P_I be the period of inhibitory inputs. Since $s_I' = -\beta_I s_I$ between inhibitory inputs, it follows that

$$s_I(t) \geq e^{-\beta_I P_I} \equiv \sigma_* \tag{10}$$

for all t.

Fig 8A shows plots of N_{lk} versus g_A when $r_E = 0$ and $s_I = \sigma_*$. Note that N_{lk} is a decreasing function of g_A and there exists g_A^0 such that $N_{lk}(\sigma_*, 0, g_A^0) = 0$. Since N_{lk} is an increasing function of r_E, it follows that if $g_A < g_A^0$, then $N_{lk}(\sigma_*, r_E, g_A) > 0$ for all $r_E > 0$. Since N_{lk} is a continuous function of s_I, it follows that if $g_A < g_A^0$ and $s_I > \sigma_*$ with $s_I - \sigma_*$ sufficiently small, then $N_{lk}(s_I, r_E, g_A) > 0$ for all r_E. In this case, the neuron is able to respond to arbitrarily low firing rates and we expect the response to inhibition to be divisive.

Fig 8B shows plots of N_{lk} versus r_E for different values of g_A when $s_I = \sigma_*$ Note that if $g_A > g_A^0$, then there exists a critical value of r_E, which we denote by $\Gamma(g_A)$, such that if $r_E < \Gamma(g_A)$, then $N_{lk}(\sigma_*, r_E, g_A) < 0$; if $r_E > \Gamma(g_A)$, then $N_{lk}(\sigma_*, r_E, g_A) > 0$. Recall that $N_{lk}(s_I, r_E, g_A)$ is a decreasing function of s_I. Hence, if $g_A > g_A^0$ and $r_E < \Gamma(g_A)$, then $N_{rk}(s_I, r_E, g_A) < 0$ for all $s_I > \sigma_*$. Moreover,

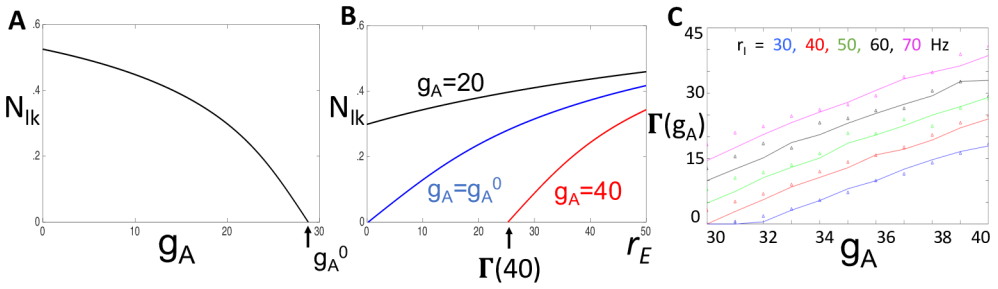

Fig 8. Identifying g_A value at the point of transition between divisive and subtractive inhibition. Dependence of the left knee, $N_{lk}(s_I, r_E, g_A)$, on **A**: g_A with $s_I = \sigma_*$ and $r_E = 0$; and **B**: r_E with $s_I = \sigma_*$ and different values of g_A. Here, $g_A^0 = 28.85$. **C**: Theoretical calculation of $\Gamma(g_A)$ (solid lines) and measured values of the minimum input rate at which solutions of the reduced model exhibits non-zero output firing rates (small triangles) for different values of the inhibitory input rate, r_I.

https://doi.org/10.1371/journal.pcbi.1006292.g008

if $g_A > g_A^0$ and $r_E > \Gamma(g_A)$ then $N_{rk}(s_I, r_E, g_A) > 0$ for $s_I > \sigma_*$ with $s_I - \sigma_*$ sufficiently small. Hence, if $g_A > g_A^0$, the neuron is not able to respond to arbitrarily low firing rates and we expect the response to inhibition to be subtractive. Given $g_A > g_A^0$, the minimum input rate at which the neuron can respond is $\Gamma(g_A)$. Fig 8C compares our theoretical calculation of $\Gamma(g_A)$ to measured values of the minimum input rate at which the reduced model exhibits non-zero output firing rates (theoretical approximation shown with solid line, simulation results shown with symbols). We report this comparison between theory and computation for values of inhibitory input rate (r_I) that vary from 30 Hz to 70 Hz in increments of 10 Hz.

Output rate approximation using dead-time modified Poisson process. The previous analysis was concerned with small output firing rates. Here we consider output rates bounded away from zero. For this analysis, we first consider the model without inhibition and discuss the impact of the refractory period on the neuron's output rate. We then discuss the impact of inhibitory inputs.

Formulation of output rate as dead-time modified Poisson process. In our simulations, we typically use excitatory inputs that are sufficiently strong so that, in the absence of refractory effects and inhibition, a single excitatory input event triggers an output spike. In response to weak excitatory inputs, the model produces low spike rates that are abolished by modest amounts of A-current, so we do not analyze the weak-input regime. At low input rates in the strong-input regime and with $g_{Syn,I} = 0$, we expect generation of output spikes to replicate the sequence of input excitatory events. Specifically, the output spike train will follow a homogeneous Poisson process with the same rate as excitatory events: $r_{out} = r_E$.

For high input rates, a refractory effect prevents the neuron from firing on a one-to-one basis with each input event. A simple approximation of the input/output relationship in this "high input rate" regime is to assume there is a fixed period of duration R ms during which the neuron cannot fire, and therefore we say

$$\text{Input event at time t} \rightarrow \begin{cases} \text{Output spike if previous spike occurred} > R \text{ in the past} \\ \text{No output spike otherwise.} \end{cases} \tag{11}$$

Since input events are drawn from a homogeneous Poisson process, the output events under this approximation follow a dead time modified Poisson process with dead time (i.e. refractory period) R. The input/output firing rate relationship is then given by

$$r_{out} = \frac{r_E}{1 + r_E R} \tag{12}$$

where rate is defined as the expected number of events a time interval, divided by the duration of that interval [26].

Definition of the firing threshold. The approximation of r_{out} introduced in Eq 12 does not incorporate any effect of inhibition. To incorporate the effects of inhibition into the formulation, we presume that excitatory input events will produce output spikes (following the dead-time modified Poisson process, as described above) unless the excitatory event occurs at a time when synaptic inhibition is sufficiently strong to prevent spiking. In other words, we define a *firing threshold* $\theta = \theta(r_E, g_A)$ to be the value of the inhibitory conductance s_I for which an excitatory input will evoke a spike only if $s_I < \theta$. For now, we assume that θ is known. Later, we describe how θ can be computed.

Suppose that inhibitory events occur periodically with period P_I. At the onset of each inhibitory event, the inhibition conductance s_I increases to 1 and then exponentially decays with

time constant $1/\beta_I$. It follows that the fraction of time that that $s_I < \theta$ is given by

$$\rho = 1 + \frac{\log \theta}{P_I \beta_I}. \tag{13}$$

By the definition of the firing threshold, this is the fraction of time that the neuron responds to excitatory input. Hence, we modify the Poisson approximation of output firing rate to be

$$r_{out} = \frac{r_E\ \rho}{1 + R r_E}. \tag{14}$$

To complete the analysis, it still remains to compute the firing threshold, θ, which depends on the parameters r_E and g_A.

Computing the firing threshold. Our derivation of the firing threshold procedes as follows. Let n_{av} be the average value of $\{n_k: k = 1, 2, \ldots\}$ such that for each k: i) there is an excitatory input at some time, t_0, with $n(t_0) = n_k$; and ii) the neuron responds to this excitatory input with a spike. We show below that if n_{av} is known, then we can compute the firing threshold, θ, while if θ is known, then we can compute n_{av}. This gives rise to two maps: $\theta = \Theta(n_{av})$ and $n_{av} = N(\theta)$. If (θ^*, n^*) is a fixed point of these two maps, then the firing threshold is given by $\theta = \theta^*$. In what follows, we make several simplifying assumptions. We compare predictions of the analysis with simulations of the reduced model later.

Suppose that n_{av} is given. Here we assume that if an excitatory input arrives at time t_0 and the neuron responds to this input with a spike, then $n(t_0) = n_{av}$. Recall that the neuron will spike in response to an excitatory input at time t_0 if $(V(t_0), n(t_0))$ lies below the left knee of $s_E = 1$ nullcline, which depends on the other variables, b and s_I. As before, let $b = b^*_{av}(r_E)$. The firing threshold can then be defined as the value of s_I so that $N_{lk}(s_I, r_E, g_A) = n_{av}$. This defines the map $\theta = \Theta(n_{av})$.

Now suppose we are somehow given the firing threshold θ and wish to estimate n_{av}. The first step is to determine the position of the right knee of the $s_E = 1$ cubic, which we denote as N_{rk}. This depends on s_I, b and g_A; however, as the dependence of N_{rk} on each of these variables is weak, we will assume that N_{rk} is a constant. We determine its value using XPPAUT.

We next consider the evolution of n in the silent phase. Here, we assume that $n_\infty(V) = 0$ and $\tau_n(V) = \tau_0$, a constant. Then, while in the silent phase, $n(t)$ satisfies $n' = -\frac{\phi_n}{\tau_0}\ n$, so that $n(t) = N_{rk}\, e^{-\frac{\phi_n\, t}{\tau_0}}$. If the firing threshold θ is known, then the output firing rate, r_{out}, is given by Eq 14. The average interspike interval is, therefore, $1000/r_{out}$ ms, which we assume is the average time the neuron spends in the silent phase. In this case, the average value of n is given by

$$n_{av} = N_{rk}\, e^{-\frac{1000\ \phi_n}{\tau_0\ r_{out}}}.$$

This defines the map $n_{av} = N(\theta)$.

We have now defined the two maps, $\theta = \Theta(n_{av})$ and $n_{av} = N(\theta)$. By taking the composition of these maps, we obtain the fixed point problem: $n = N \circ \Theta(n)$. This map is continuous in n, and n takes values in the closed interval [0, 1], so there exists a fixed-point of this map [27]. We use successive iterations of the bisection method to numerically compute n_{av} as the solution of the fixed point fixed point problem $n = N \circ \Theta(n)$, and then set $\theta = \Theta(n_{av})$.

Slope of output rates at onset of firing in the divisive case. By computing the firing threshold at $r_E = 0$, we can study the behavior of the model near the onset of firing. In particular, if g_A is sufficiently small or $g_{Syn,E}$ is sufficiently large, then inhibition is divisive and the neuron is able to fire in response to arbitrarily low firing rates (recall Fig 2). Our goal here is to compute the slopes of the input/output firing rate curves at $r_E = 0$ in the case of divisive inhibition.

This is done by simply differentiating the firing rate approximation in Eq 14 with respect to r_E and setting $r_E = 0$. This yields

$$r'_{out}(0) = 1 + \frac{\log \theta_0}{P_I \beta_I} \tag{15}$$

where θ_0 is the firing threshold when $r_E = 0$. This can be easily computed using XPPAUT as follows. Since we are considering arbitrarily low firing rates, it follows that the average value of n at times of output spikes is $n_{av} \approx 0$, where n_{av} was defined in the preceding section. The analysis in that section demonstrates that $\theta_0 = \Theta(0)$, i.e. it is the value of s_I so that $N_{lk}(s_I, 0, g_A) = 0$.

In Fig 9, we plot the slope of the input/output firing rate curves at $r_E = 0$ computed from both the theoretical prediction (Eq 15) and simulations of the full model. There is a tendency for the approximated value of the slope at firing onset to overestimate the slope computed in simulations of the full model. Nonetheless, the theory captures qualitative features of the relationship between slope at firing rate onset and A-channel conductance. In particular, the slope at firing rate onset decreases as g_A increases, indicating gain control by inhibition is "stronger" with higher values of g_A. The value of g_A at which the slope reaches zero (g_A between 25 and 30) was denoted as g_A^0 previously; it is the critical value of g_A at which the effect of inhibition switches from divisive to subtractive.

Approximation of output rates at arbitrary input rates. To more completely characterize output firing rates, we seek to extend our approximations to cases of higher output rates. In other words, we consider the firing rate equation (Eq 14) for $r_E > 0$. We previously described how to compute θ. With θ known, the only undetermined parameter in the firing rate equation is R. We interpret this parameter as the duration of the refractory period in the model. The value

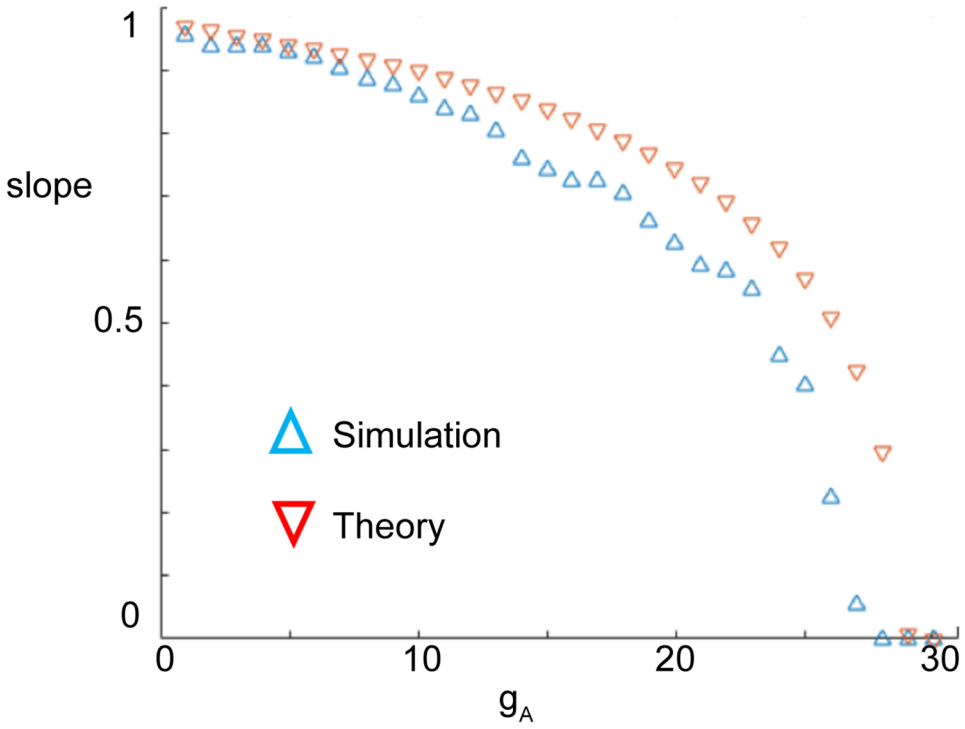

Fig 9. The slope of the input/output firing rate curves at $r_E = 0$ computed from both the theoretical prediction Eq 15 and simulations of the full model.

https://doi.org/10.1371/journal.pcbi.1006292.g009

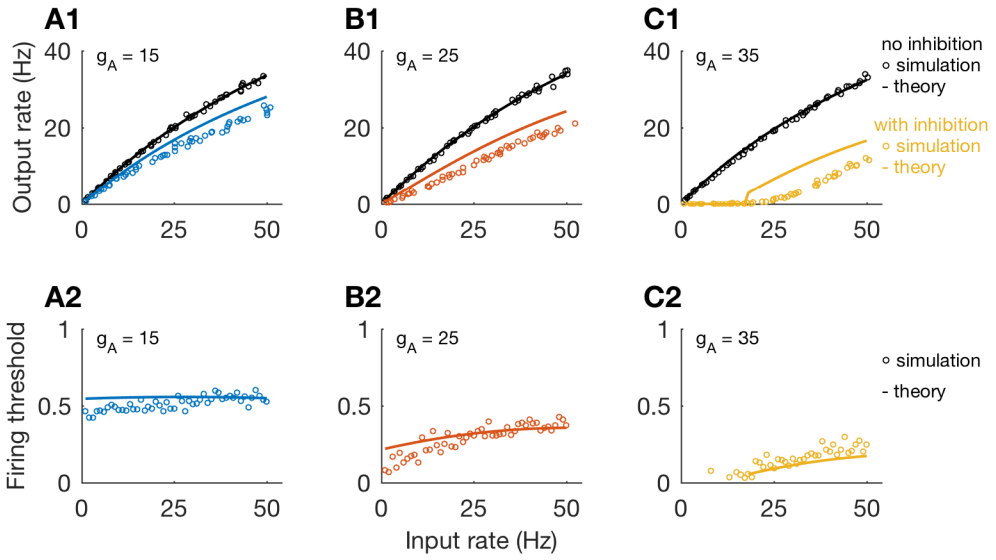

Fig 10. Output firing rates approximated as dead-time modified Poisson process with firing threshold. Top row: Firing rate as a function of input rate obtained from simulations (circles) and theoretical approximation (lines); for $g_A = 15$ (A1), $g_A = 25$ (B1), and $g_A = 35$ (C1). Simulations and theory show transition from divisive to subtractive inhibition as g_A increases. **Bottom row**: Theoretical approximation of firing threshold θ (lines), and the largest observed values of s_I for which excitatory inputs elicited spikes in simulations (circles), plotted as functions of input rate; for $g_A = 15$ (A2), $g_A = 25$ (B2), and $g_A = 35$ (C2).

https://doi.org/10.1371/journal.pcbi.1006292.g010

of R depends on the internal dynamics of the model, strength of excitatory inputs, and other factors. To obtain approximations for R, we simulated firing rate input/output curves (without inhibition) and performed a nonlinear curve-fit using Eq 12 to estimate its value. We find that $R \approx 10$ ms (with some dependence on g_a) provides accurate approximations to the firing rate functions in the absence of inhibition.

We compare our theoretical approximation to the firing rate of the model neuron to simulated firing rates in Fig 10. The dead-time modified Poisson process provides a satisfactory description of firing rate responses without inhibition (black, top row), for various values of g_A (values of g_A increase from 15 to 35, in increments of 10, from left-to-right in this figure). When we include inhibition in these simulations, we find that the approximated firing rate (using the firing rate threshold computation outlined above) tends to overestimate simulated firing rates (colors). Nevertheless, approximations do capture the qualitative differences in firing rate curves for divisive inhibition (smaller values of g_A) and subtractive inhibition (larger values of g_A).

The firing threshold calculation defines θ, the theoretical value of s_I for which the neuron cannot produce a spike if an incoming excitatory event arrives at a time when $s_I \geq \theta$. We plot values of θ as colored lines in the lower row of Fig 10. To compare θ to simulations, we recorded the values of s_I at the time of every excitatory event that triggered a spike. Then, for each input rate (x-axis), we found the maximum value of s_I for these spike-triggering excitatory events. These maximum s_I values qualitatively align with our approximations of θ, further supporting the heuristic concept of a firing threshold.

We point out that, following from Eqs 12 and 14 that a "purely divisive" response would be one for which the firing threshold is constant with respect the input rate. This can (nearly) occur for specific parameter sets; see for instance the nearly constant threshold in Fig 10A2. However, firing threshold depends in general on input rate. Furthermore, a "purely subtractive" response would be one for which the firing threshold is piecewise constant (a step

function). The firing threshold in Fig 10C2 increases with input rate in a non-monotonic fashion, so inhibition in this case, in fact, has both divisive and subtractive characteristics. This is true in general and we reiterate that our use of the term "subtractive" encompasses cases for which inhibition has both divisive and subtractive effects.

Results for non-instantaneous A-current activation

A key assumption in the formulation and analysis of the reduced model is that the A-current activates sufficiently fast so that the dynamical variable a can be set to its voltage-dependent steady state value; that is, we set $a = a_\infty(V)$. One effect of this change from a evolving dynamically with $\tau_a = 2$ ms (the full model), to a evolving instantaneously as $a_\infty(V)$ (the reduced model), is that excitation must be much stronger in the reduced model to observe subtractive inhibition. Typical values of $g_{Syn,E}$ in the full model are around 0.5 (see Fig 4), and typical values of $g_{Syn,E}$ in the reduced model are around 3. This suggests that the speed of A-current activation (not just the strength of the A-current) plays a role in switching the effect of inhibition from divisive to subtractive.

For inhibition to have a subtractive effect, responses to infrequent excitatory inputs must be suppressed. In the reduced model, this occurs when g_A is sufficiently strong because the A-type channel activates "instantaneously" and can prevent spike initiation. In the one-compartment model with "non-instantaneous" a variable, large g_A could switch the effect of inhibition to subtractive, but only if excitatory input strength was also sufficiently small (recall Fig 4). The importance of small $g_{Syn,E}$ is demonstrated in Fig 11. We show time-courses of voltage in the one-compartment model for $g_{Syn,E} = 0.2$, 0.5, and 1, and with $g_A = 0$ and $g_I = 0$. In all cases, the input evokes an output spike. Notice, however, that as input strength weakens, there is a marked delay in the time before spike initiation. For the weakest input used ($g_{syn,E} = 0.2$), there is a delay of roughly 2 ms before the rapid upstroke of V at the onset of the action potential. During this "pause", voltage is slowly ramping up and, simultaneously, recruiting additional A-current as the a variable activates. The amount of I_A available to suppress spike initiation depends, therefore, on A-channel maximal conductance (g_A) and also the time-constant of I_A activation (τ_A).

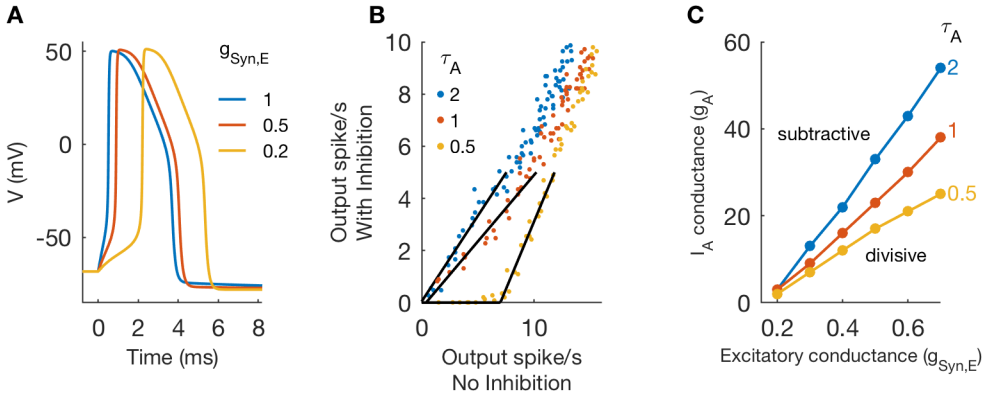

Fig 11. Role of τ_A in determining switch between divisive and subtractive inhibition. A: Voltage traces in response to excitatory inputs of varying strengths ($g_A = 0$, and $g_{Syn,I} = 0$). **B**: Threshold-linear relation between output firing rates in simulations of one-compartment model with and without inhibition for varying A-channel activation time constant ($\tau_A = 0.5, 1, 2$) and $g_A = 20$. Synaptic parameter values are $g_{Syn,E} = 0.5$, and (for simulations with inhibition) $g_{Syn,I} = 1$ and $r_I = 50$. **C**: Critical values of g_A that define boundary between subtractive and divisive inhibition in ($g_{Syn,E}$, g_A) parameter space. The boundary shifts downward as τ_A decreases, indicating that faster activating A-current enables inhibition to have a subtractive effect for lower values of g_A.

https://doi.org/10.1371/journal.pcbi.1006292.g011

From this observation, we draw the following conclusion: "non-instantaneous" I_A can act to switch the effect of inhibition from divisive to subtractive, but only if it activates rapidly enough relative to the dynamics of spike initiation. To illustrate our point, we simulated the model with three values of A-channel activation time constant (τ_A = 0.5, 1, 2), using $g_{Syn,E}$ = 0.5, $g_{Syn,I}$ = 1, and r_I = 50 Hz. As shown in Fig 11B, inhibition is divisive for slower activation kinetics (τ_A = 1, 2) and subtractive for faster activation kinetics (τ_A = 0.5). In Fig 11C, we map the boundary between divisive and subtractive inhibition in the ($g_{Syn,E}$, g_A) parameter plane. There is a strong effect of τ_A. Faster activation kinetics (smaller τ_A values) shift the critical point at which inhibition switches from divisive to subtractive to lower values values of g_A.

Results for multi-compartment model

Our prior observation, that delaying spike initiation allows inhibition to have a subtractive effect for "non-instantaneous" A-channel activation, led us to investigate other cellular mechanisms that could have a similar effect. To this end, we considered a multi-compartment neuron model that describes a soma and passive dendrite. Inhibition and voltage-gated currents are restricted to the soma compartment, and excitation targets a location somewhere on the dendrite. Passive cable theory tells us that the amplitudes of excitatory post-synaptic potentials attenuate and their rising slopes become less steep as signals spread along the cable [28]. By varying the location of excitatory synaptic inputs to the dendrite in the multi-compartment model, we can, therefore, adjust the shape of excitatory post-synaptic potentials as they arrive in the soma.

Examples of action potentials, recorded in the soma compartment, in response to inputs at different locations along the dendrite are shown in Fig 12A. Synaptic conductance strength is constant ($g_{Syn,E}$ = 2 in these simulations). Inputs that arrive proximal to the soma are large and fast-rising relative to responses to more distal inputs, and thus evoke action potentials with shorter latencies. The parameter cpt_{in} identifies the compartment that receives synaptic excitation. It takes values from 1 (proximal) to 9 (distal).

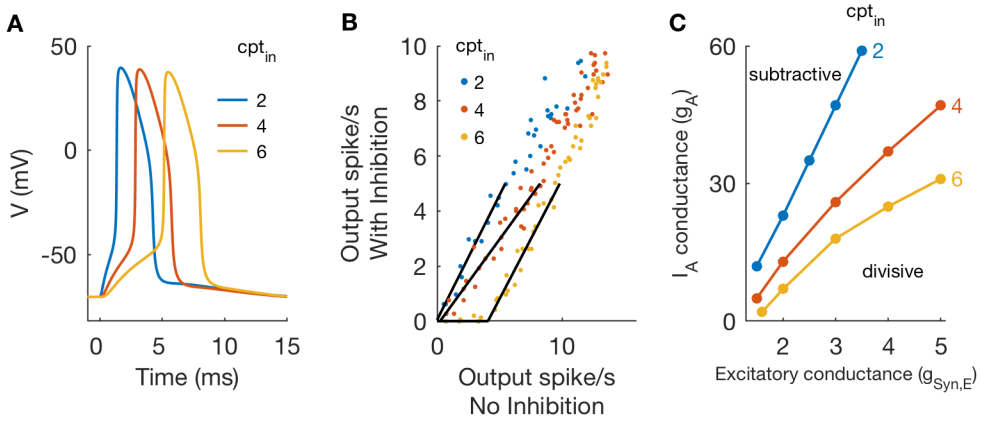

Fig 12. Divisive and subtractive inhibition in a multi-compartment neuron model. A: Voltage traces in response to excitatory inputs at varying input locations along the dendrite. Parameter values in these simulations: $g_{Syn,E}$ = 3, $g_{Syn,I}$ = 0, and g_A = 0. Inputs distant from the soma lead to spike initiation with millisecond-scale delay between excitatory input and spike onset. **B**: Threshold-linear relation between output firing rates in simulations of the multi-compartment model with and without inhibition for varying input location and g_A = 20. For simulations with inhibition: $g_{Syn,I}$ = 1 and r_I = 50. Inhibition is subtractive for distal excitatory input (cpt_{in} = 6). **C**: Critical values of g_A that define boundary between subtractive and divisive inhibition in ($g_{Syn,E}$, g_A) parameter space. The boundary shifts downward as excitatory inputs are moved to more distal locations, indicating that inhibition has a subtractive effect for lower values of g_A for more distal inputs.

https://doi.org/10.1371/journal.pcbi.1006292.g012

We included synaptic inhibition in the model targeting the soma, and used simulations to characterize the effect of inhibition as either subtractive or divisive. In Fig 12B we observe a transition from divisive to subtractive inhibition as we move the location on the dendrite at which synaptic excitation targets the cell. This matches our expectation: synaptic excitation placed at more distant locations will generate weaker and slower rising inputs in the soma. This will, in turn, lead to spikes that initiate slowly and that give time for A-channel conductance to activate and prevent spike generation. In additional simulations included as S4 Fig we targeted inhibitory inputs to the dendrite and did not observe substantially different results.

We explored the (g_A, $g_{Syn,E}$) parameter plane and identified the boundary separating regions in which inhibition has a divisive effect on firing rates and regions in which inhibition has a subtractive effect (following the procedure used previously for Fig 4). We find that there is a dramatic effect of input location, as shown in Fig 12C. The region of the (g_A, $g_{Syn,E}$) parameter plane over which inhibition has a divisive effect is smaller when inputs are more distant from the soma.

Discussion

Neurons process and convey information in the brain by converting barrages of synaptic inputs into spiking outputs. This transfer from inputs to outputs is a highly complex process due to the inherently noisy and nonlinear nature of synaptic and neural processes. Using a combination of computer simulation and mathematical analysis of biophysically-based neuron models, we have probed the relation between synaptic inputs and spiking outputs. We found that the A-type potassium current (a fast-activating, negative feedback current) can act to switch the effect of inhibition on output firing from divisive to subtractive. This provides a clear demonstration of how the internal dynamics of a neuron can control the functional impact of inhibition.

Analysis identifies when I_A promotes divisive or subtractive inhibition

Using simulations and phase plane analysis, we systematically investigated conditions under which inhibition acts on firing rate outputs in a divisive or subtractive manner. We first identified critical values of I_A conductance (g_A) at which the effect of inhibition switched from divisive (for lower g_A values) to subtractive (for higher g_A values) (Fig 4). In the reduced model, we approximated this critical value of g_A using bifurcation analysis. By tracking the left-knee of the V-nullcline (Fig 5), we identified this critical value of g_A as a bifurcation point at which the neuron model ceased to be excitable in response to synaptic inputs (Fig 8). Key in this analysis was the separation of time scales between fast variables (V) and slow variables (n, b). In fact, the inactivation variable b was sufficiently slow that it could be treated as a constant with a value that depended on the input rate (Fig 7). This simplification enabled further analysis. By viewing the spiking output of the model as a Poisson process modified by a refractory period and inhibition-dependent firing threshold, we approximated firing rates at the point of spiking onset (Fig 9) as well as for arbitrary input rates (Fig 10).

A-type potassium current is a source of dynamic, voltage-gated negative feedback that is fast activating. We leveraged this property to obtain analytical results by assuming that the gating variable for I_A activation, a, evolved instantaneously to its voltage-dependent equilibrium value (see also [23]). We also performed simulations without this assumption and discovered a delicate interaction between the speeds of I_A activation and spike initiation. In particular, subtractive inhibition required that I_A is sufficiently strong and that it activates sufficiently rapidly to prevent spike initiation (Fig 11). For our standard value of I_A activation (τ_A = 2 ms), we found that, in conditions of slow spike initiation, I_A could "ramp up" during slowly-developing

spikes and suppress spike initiation. Weak excitatory inputs, or excitatory inputs targeting more distal regions in a model that included a spatially-extended dendritic process (Fig 12) produced spikes that were slow to initiate, and were therefore scenarios in which inhibition was subtractive for low to modest levels of g_A.

Relation to previous works

Divisive inhibition is a mechanism of neural gain control and has been the subject of numerous studies; see [1] for review. We found that, at lower levels of g_A, inhibition can have a divisive effect on the input/ouput properties of a spiking neuron responding to a mixture of random excitatory inputs and periodic inhibitory inputs. The amount of g_A altered the slope (gain) of the output firing rate, and thereby tunes the gain control in this system. This result is consistent with the results of a recent *in vitro* study of neurons in the rostral nucleus of the solitary tract [24]. In that experiment, Chen and colleagues controlled inhibition using optogenetic techniques and constructed threshold linear functions to express the relation between firing responses with and without inhibition (analogous to our Fig 2C, and similar figures). They observed that slopes of threshold-linear function were more shallow for neurons with I_A, as compared to neurons in the same nucleus that did not have I_A. Thus, the presence of I_A enhanced the divisive effect of inhibition. Previous modeling work has identified similar gain control effects by I_A [29].

We observed, additionally, that at higher levels of g_A, the A-type current can switch the effect of inhibition from divisive to subtractive. This demonstrates a novel example of how the internal dynamics of a neuron interact with synaptic inhibition to change the neuron's computational properties (input/output relation). Previous studies have explored the multi-faceted ways in which I_A current can alter neural dynamics. Connor and Stevens established I_A current as a mechanism to prolong interspike intervals of repetitively-firing neurons to arbitrary lengths ("type I" firing dynamics) [11]. Other identified functions of I_A include prolonging first spike latency [30], producing burst firing patterns and preventing anodal break (rebound) firing [23], filtering synaptic inputs in favor of slow time-scale NMDA receptor-mediated inputs [31], and affecting the correlation in spiking among neurons responding to common inputs [32]. Our contribution adds to the rich repertoire of I_A function.

Implications for modulation of inhibitory effects

We have identified routes to subtractive inhibition that depends only on mechanisms that could be readily adjusted by processes of plasticity and neuromodulation. In particular, we have shown that strong and fast I_A can lead to subtractive inhibition. The strength and kinetics of the A-type Potassium channels can be modulated in a variety of ways [33–36]. For example, in neurons involved in gastro-intestinal function, A-type potassium channels were modified both by diet [37–39] and gastric disorders [40].

We also found that weak excitatory inputs or more distally-located excitatory inputs led to subtractive inhibition by slowing the onset of action potentials. Synaptic plasticity and modulation of the electrical properties of dendrites can adjust the strength and propagation of excitatory inputs [41], and plasticity of spike initiation zones could change the dynamics of spike initiation [42, 43]. These changes happen at the level of the output neuron. They do not require "global" modulatory effects to change background network activity, circuit structure, or the balance of excitation and inhibition. We conclude, then, that I_A can add flexibility to neural systems by allowing neurons to "self-regulate" whether inhibition acts in a subtractive or divisive manner.

Supporting information

S1 Fig. Examples of divisive and subtractive effects of inhibition in the one-compartment model with randomly-timed inhibitory inputs (homogeneous Poisson process). A, B: Output firing rates as a function of excitatory input rate, computed from simulations without inhibition (empty circles, $g_{Syn,I} = 0$) and with inhibition (filled circles, $g_{Syn,I} = 1$ and $r_I = 50$ Hz). Excitatory synaptic strength is $g_{Syn,E} = 0.5$. In **A**: Divisive rescaling of the input/output relation with $g_A = 20$. In **B**: Subtractive shifting of the input/output relation with $g_A = 40$. **C**: Data from **A** and **B** are replotted with output firing rates in the absence of inhibition on the ordinate and output firing rates in the presence of inhibition on the abscissa. Threshold-linear functions are fit to simulation data (black lines). Rightward shift of threshold-linear function for $g_A = 40$ is characteristic of subtractive inhibition.
(TIF)

S2 Fig. Boundary between subtractive and divisive inhibition in ($g_{Syn,E}$, g_A) parameter space using randomly-timed inhibition (Poisson process with rate r_I). A, B: For each parameter set, we fit threshold-linear functions to characterize the relationship between output firing rates in the presence and absence of inhibition. Dots in each panel identify the smallest value of g_A (for a given parameter set) at which inhibition is subtractive. In **A**: We vary inhibition strength ($g_{Syn,I} = 0.5, 1, 2$) and keep inhibition rate fixed at 50 Hz. In **B**: We vary inhibition rate ($r_I = 30, 50, 70$ Hz) and keep inhibition strength fixed at $g_{Syn,I} = 1$. The values of g_A that define the boundary between subtractive and divisive inhibition decrease with increases in either inhibition parameter ($g_{Syn,I}$ or r_I).
(TIF)

S3 Fig. Examples of "mixed" divisive and subtractive effects of inhibition in the one-compartment model with periodic inhibitory inputs. Inpout/output firing rate relations for varying A-channel conductance. Inhibition is divisive for lower g_A (compare slopes for $g_A = 0$ and $g_A = 20$), and shows both divisive and subtractive features for higher values of g_A (notice rightward-shift of input/output curves, but also changes in slopes indicated in legend). We classify as *subtractive* any response for which the input/output curve is shifted rightward. Thus, subtractive responses (in our classification) also include "mixed" responses such as those shown here.
(TIF)

S4 Fig. Divisive and subtractive inhibition in a multi-compartment neuron model with inhibition that targets sites on the dendrite of the multi-compartment model. A: Threshold-linear relations between output firing rates in simulations of the multi-compartment model with and without inhibition for varying inhibition input location and $g_A = 20$. For simulations with inhibition: $g_{Syn,I} = 1$ and $r_I = 50$. Inhibition is divisive for inhibitory inputs that target the soma ($cpt_{inhib} = 0$), an intermediate position on the dendrite ($cpt_{inhib} = 4$, same as locatioin of excitatory input), and a distal location on the dendrite ($cpt_{inhib} = 8$). **B**: Threshold-linear relations for varying inhibition input location and $g_A = 30$. For simulations with inhibition: $g_{Syn,I} = 1$ and $r_I = 50$. Inhibition is subtractive for inhibitory inputs that target the soma or positions on the dendrite.
(TIF)

S1 Dataset. Dataset for figures. Excel data set containing data used to produce figures.
(XLSX)

Acknowledgments

The authors thank Xueying Wang for helpful discussions and insights.

Author Contributions

Conceptualization: Joshua H. Goldwyn, Joseph B. Travers, David Terman.

Data curation: Joshua H. Goldwyn.

Formal analysis: Joshua H. Goldwyn, David Terman.

Investigation: Joshua H. Goldwyn, Bradley R. Slabe, David Terman.

Methodology: Joshua H. Goldwyn, David Terman.

Software: Joshua H. Goldwyn.

Visualization: Joshua H. Goldwyn, Bradley R. Slabe, David Terman.

Writing – original draft: Joshua H. Goldwyn, David Terman.

Writing – review & editing: Joshua H. Goldwyn, Joseph B. Travers, David Terman.

References

1. Silver RA. Neuronal arithmetic. Nature Reviews Neuroscience. 2010; 11(7):474–489. https://doi.org/10.1038/nrn2864 PMID: 20531421
2. Wilson NR, Runyan CA, Wang FL, Sur M. Division and subtraction by distinct cortical inhibitory networks in vivo. Nature. 2012; 488(7411):343–348. https://doi.org/10.1038/nature11347 PMID: 22878717
3. Doiron B, Longtin A, Berman N, Maler L. Subtractive and Divisive Inhibition: Effect of Voltage-Dependent Inhibitory Conductances and Noise. Neural Computation. 2001; 13(1):227–248. https://doi.org/10.1162/089976601300014691 PMID: 11177434
4. Chance FS, Abbott LF, Reyes AD. Gain modulation from background synaptic input. Neuron. 2002; 35(4):773–782. https://doi.org/10.1016/S0896-6273(02)00820-6 PMID: 12194875
5. Prescott SA, De Koninck Y. Gain control of firing rate by shunting inhibition: Roles of synaptic noise and dendritic saturation. Proceedings of the National Academy of Sciences. 2003; 100(4):2076–2081. https://doi.org/10.1073/pnas.0337591100
6. Mitchell SJ, Silver RA. Shunting inhibition modulates neuronal gain during synaptic excitation. Neuron. 2003; 38(3):433–445. https://doi.org/10.1016/S0896-6273(03)00200-9 PMID: 12741990
7. Rothman JS, Cathala L, Steuber V, Silver RA. Synaptic depression enables neuronal gain control. Nature. 2009; 457:1015–1018. https://doi.org/10.1038/nature07604 PMID: 19145233
8. Mejias JF, Payeur A, Selin E, Maler L, Longtin A. Subtractive, divisive and non-monotonic gain control in feedforward nets linearized by noise and delays. Frontiers in Computational Neuroscience. 2014; 8:19. https://doi.org/10.3389/fncom.2014.00019 PMID: 24616694
9. Gu C, Barry J. Function and mechanism of axonal targeting of voltage-sensitive potassium channels. Progress in Neurobiology. 2011; 94:115–132. https://doi.org/10.1016/j.pneurobio.2011.04.009 PMID: 21530607
10. Vacher H, Mohapatra D, Trimmer J. Localization and targeting of voltage-dependent ion channels in mammalian central neurons. Physiological Review. 2008; 88(4):1407–1447. https://doi.org/10.1152/physrev.00002.2008
11. Connor JA, S CF. Prediction of repetitive firing behaviour from voltage clamp data on an isolated neurone soma. The Journal of Physiology. 1971; 213(1):31. https://doi.org/10.1113/jphysiol.1971.sp009366 PMID: 5575343
12. Jerng H, Pfaffinger P, Covarrubias M. Molecular physiology and modulation of somatodendritic A-type potassium channels. Mol Cell Neursoci. 2004; 27(4):343–369. https://doi.org/10.1016/j.mcn.2004.06.011
13. Shi W, Wymore RS, Wang HS, Pan Z, Cohen IS, McKinnon D, et al. Identification of two nervous system-specific members of the erg potassium channel gene family. Journal of Neuroscience. 1997; 17(24):9423–9432. https://doi.org/10.1523/JNEUROSCI.17-24-09423.1997 PMID: 9390998

14. Strube C, Saliba L, Moubarak E, Penalba V, Martin-Eauclaire MF, Tell F, et al. Kv4 channels underlie A-currents with highly variable inactivation time courses but homogeneous other gating properties in the nucleus tractus solitarii. Pflugers Arch. 2015; 467(4):789–803. https://doi.org/10.1007/s00424-014-1533-z PMID: 24872163

15. Trimmer J, Rhodes K. Localization of voltage-gated ion channels in mammalian brain. Annual Review of Physiology. 2004; 66:477–519. https://doi.org/10.1146/annurev.physiol.66.032102.113328 PMID: 14977411

16. Na Phuket T, Covarrubias M. Kv4 channels underlie the subthreshold-operating A-type K-current in nociceptive dorsal root ganglion neurons. Frontiers in Molecular Neuroscience. 2009; 2:3. https://doi.org/10.3389/neuro.02.003.2009

17. Kloppenburg P, Levini RM, Harris-Warrick RM. Dopamine modulates two potassium currents and inhibits the intrinsic firing properties of an identified motor neuron in a central pattern generator network. Journal of Neurophysiology. 1999; 81(1):29–38. https://doi.org/10.1152/jn.1999.81.1.29 PMID: 9914264

18. Sonner P, Sterrn J. Functional role of A-type potassium currents in rat presympathetic PVN neurones. Journal of Physiology. 2007; 582(3):1219–1238. https://doi.org/10.1113/jphysiol.2007.134379 PMID: 17525115

19. Hille B. Potassium Channels and Chloride Channels. In: Ionic Channels of Excitable Membranes. 2nd ed. Sinauer Associates; 1992.

20. Izhikevich E. Conductance-Based Models and Their Reductions. In: Dynamical Systems in Neuroscience. MIT; 2007.

21. Levitan IB. Modulation of ion channels in neurons and other cells. Annual Review of Neuroscience. 1988; 11(1):119–136. https://doi.org/10.1146/annurev.ne.11.030188.001003 PMID: 2452594

22. Rinzel J. On repetitive activity in nerve. Federation Proceedings. 1978; 37(14):2793–2802. PMID: 720633

23. Rush ME, Rinzel J. The potassium A-current, low firing rates and rebound excitation in Hodgkin-Huxley models. Bulletin of Mathematical Biology. 1995; 57(6):899–929. https://doi.org/10.1016/S0092-8240(95)80006-9 PMID: 8528161

24. Chen Z, Travers SP, Travers JB. Inhibitory modulation of optogenetically identified neuron subtypes in the rostral solitary nucleus. Journal of Neurophysiology. 2016; 116(2):391–403. https://doi.org/10.1152/jn.00168.2016 PMID: 27146980

25. Ermentrout B. Simulating, Analyzing, and Animating Dynamical Systems. Society for Industrial and Applied Mathematics; 2002.

26. W Müller J. Some formulae for a dead-time-distorted poisson process. Nuclear Instruments and Methods. 1974; 117(2):401–404. https://doi.org/10.1016/0029-554X(74)90283-3

27. Crossley MD. Essential Topology. London: Springer London; 2010.

28. Rinzel J, Rall W. Transient response in a dendritic neuron model for current injected at one branch. Biophysical Journal. 1974; 14(10):759–790. https://doi.org/10.1016/S0006-3495(74)85948-5 PMID: 4424185

29. Patel AX, Murphy N, Burdakov D. Tuning Low-Voltage-Activated A-Current for Silent Gain Modulation. Neural computation. 2012; 24(12):3181–3190. https://doi.org/10.1162/NECO_a_00373 PMID: 22970874

30. Gerber B, Jakobsson E. Functional significance of the A-current. Biological Cybernetics. 1993; 70(2):109–114. https://doi.org/10.1007/BF00200824 PMID: 8312402

31. Schoppa NE, Westbrook GL. Regulation of synaptic timing in the olfactory bulb by an A-type potassium current. Nature Neuroscience. 1999; 2(12):1106–1113. https://doi.org/10.1038/16033 PMID: 10570488

32. Barreiro AK, Thilo EL, Shea-Brown E. A-current and type I/type II transition determine collective spiking from common input. Journal of Neurophysiology. 2012; 108(6):1631–1645. https://doi.org/10.1152/jn.00928.2011 PMID: 22673330

33. Birnbaum SG, Varga AW, Yuan LL, Anderson AE, Sweatt JD, Schrader LA. Structure and function of Kv4-family transient Potassium channels. Physiological Reviews. 2004; 84(3):803–833. https://doi.org/10.1152/physrev.00039.2003 PMID: 15269337

34. An WF, Bowlby MR, Betty M, Cao J, Ling HP, Mendoza G, et al. Modulation of A-type potassium channels by a family of calcium sensors. Nature. 2006; 403:553–556. https://doi.org/10.1038/35000592

35. Cai SQ, Li W, Sesti F. Multiple modes of A-type Potassium current regulation. Current Pharmaceutical Design. 2007; 13(31):3178–3184. https://doi.org/10.2174/138161207782341286 PMID: 18045167

36. Carrasquillo Y, Nerbonne JM. IA channels: Diverse regulatory mechanisms. The Neuroscientist. 2014; 20(2):104–111. https://doi.org/10.1177/1073858413504003 PMID: 24106264

37. Boxwell AJ, Chen Z, Mathes CM, Spector AC, Roux CWL, Travers SP, et al. Effects of high-fat diet and gastric bypass on neurons in the caudal solitary nucleus. Physiology & Behavior. 2015; 152:329–339. https://doi.org/10.1016/j.physbeh.2015.07.025

38. Browning KN, Fortna SR, Hajnal A. Roux-en-Y gastric bypass reverses the effects of diet-induced obesity to inhibit the responsiveness of central vagal motoneurones. The Journal of Physiology. 2013; 591(9):2357–2372. https://doi.org/10.1113/jphysiol.2012.249268 PMID: 23459752

39. Li S, Maude-Griffin R, Pullan AJ, Chen ZJD. Gastric emptying and Ca2+ and K+ channels of circular smooth muscle cells in diet-induced obese prone and resistant rats. Obesity. 2013; 21(2):326–335. https://doi.org/10.1002/oby.20021 PMID: 23404843

40. Li S, Chen JDZ. Down-regulation of A-type potassium channel in gastric-specific DRG neurons in a rat model of functional dyspepsia. Neurogastroenterology & Motility. 2014; 26(7):962–970. https://doi.org/10.1111/nmo.12350

41. Sjostrom PJ, Rancz EA, Roth A, Hausser M. Dendritic excitability and synaptic plasticity. Physiological Reviews. 2008; 88(2):769–840. https://doi.org/10.1152/physrev.00016.2007 PMID: 18391179

42. Adachi R, Yamada R, Kuba H. Plasticity of the axonal trigger zone. The Neuroscientist. 2015; 21(3):255–265. https://doi.org/10.1177/1073858414535986 PMID: 24847046

43. Brette R. Sharpness of spike initiation in neurons explained by compartmentalization. PLoS Computational Biology. 2013; 9(12):1–10. https://doi.org/10.1371/journal.pcbi.1003338